DOI: 10.31534/engmod.2023.2.ri.02v
Original scientific paper
Received: 16.11.2022.

Theoretical Study of the Force Parameters of the ECAP-Linex Combined Process

Evgeniy Panin[1], Irina Volokitina[2], Andrey Volokitin[1], Abdrakhman Naizabekov[2], Gulzhainat Akhmetova[1], Sergey Lezhnev[2], Andrey Tolkushkin[3], Aibol Esbolat[1]

[1] *Metal forming department, Karaganda Industrial University, Temirtau, KAZAKHSTAN*
e-mail: ye.panin@tttu.edu.kz

[2] *Metallurgy and mining department, Rudny Industrial Institute, Rudny, KAZAKHSTAN*

[3] *Metal forming department, Ural Federal University, Yekaterinburg, RUSSIA*

SUMMARY

The paper presents theoretical studies of a new deformation process combining the stages of equal-channel angular pressing (ECAP) and the Linex scheme. To analyse the resulting deformation forces, the stages of pressing in a matrix and compression by a chain conveyor are separately considered. Equations were provided for determining the forces acting on the drive pulley, ECA matrix, and chain element link. A trial calculation and comparative analysis with the previously known rolling-ECAP process showed that the new ECAP-Linex process allows for a stable deformation process with lower forces and a smaller channel junction angle in the matrix. The values obtained by equations are verified with computer simulation using the finite element method in the Deform program. A comparison of values showed that the force values in the calculation and simulation have a high level of convergence. For all three considered parameters, the difference value did not exceed 3%.

KEY WORDS: *severe plastic deformation; equal-channel angular pressing; Linex, combined process; force equation; simulation.*

1. INTRODUCTION

Over the past three decades, a large number of metal-forming methods have been developed and investigated, allowing to obtain blanks with an ultrafine-grained structure. These methods are based on various schemes of shear or alternating strains. Processes representing a simultaneous combination of shear and alternating strains are separate categories. All these processes make it possible to implement a special type of pressure treatment called severe plastic deformation (SPD).

High-pressure torsion is one of the oldest methods for obtaining bulk ultrafine-grained and nanostructured samples [1-3]. The samples obtained by this method have the shape of disks. The sample is clamped between the punch and the caliper and compressed under an applied

pressure of several *GPa*. When the caliper rotates, the surface friction forces cause the sample to deform according to the shear pattern. The bulk of the material is deformed under quasi-hydrostatic compression under the applied pressure and pressure from the outer layers of the sample. As a result, despite the high degree of strain, the deformable sample does not collapse. In this case, the deformation of the sample has a radial inhomogeneity which can be minimized with a large number of revolutions. Using the method of torsion under high pressure in various materials, it is possible to obtain a structure with a grain size of up to *20 nm*. However, the prospects for using high-pressure torsion as an industrial method have significant disadvantages because of the small size of the workpieces processed and low tool resistance due to high loads. This fact seriously narrows the practical application of this method and limits it to laboratory conditions.

The method of equal-channel angular pressing (ECAP) is devoid of many of these disadvantages and allows to obtain samples of square or rectangular cross-sections with a homogeneous ultrafine-grained structure with a grain size of *100-200 nm* and does not require complex equipment. The method consists in pushing the workpiece through the angular channel of the matrix and implementing a simple shift scheme. The technology of ECAP and its various variations are considered in [4-7]. Among the new directions in ECAP is the processing of hard-to-form materials. Experimental and theoretical modeling of the mechanics of ECAP, associated with studies of the stress-strain state, contact stresses, and friction conditions, made it possible to design tooling for obtaining large-sized blanks from various metals, such as copper, titanium, tungsten, aluminum, and their numerous alloys [8-11].

In addition to the considered SPD processes, which make it possible to obtain small-sized blanks, severe plastic deformation processes are actively developing to enable the processing of massive blanks. These methods are based on the intensification of shear and alternating strains in forging processes [12-16]. As a result, the initial billets in the form of ingots receive a high level of processing leading to intensive grain refinement throughout the cross-section. In comparison to the use of classic flat strikers, the use of new deforming tool designs due to intensive shear strain also reduces energy consumption.

Despite the fact that the severe plastic deformation processes are an effective way of crystal grain refinement [17-21], most of these methods are used only in laboratory conditions. The main disadvantages of these technologies are the lack of continuity or the inability to process long workpieces. Attempts have been made to circumvent these limitations by developing combined processes where two or more discrete processes are combined. In particular, combined processes such as ECAP-drawing, for the production of wire from ferrous and non-ferrous metals [22]; rolling-ECAP, for the production of aluminum rods of square and rectangular cross-section [23]; helical rolling-ECAP, for the production of round bars from ferrous and non-ferrous metals [24] are developed and experimentally investigated. Various types of combinations of rolling and extrusion have also been developed, including combining with the casting stage to produce rods from aluminum alloys [25, 26]. These methods have proven themselves well both in terms of the efficiency of metal processing and deformation productivity. Therefore, the development of new combined deformation processes is one of the most promising areas in metal forming.

In work [27], new concepts of combined metal forming processes are proposed, one of which is the ECAP – Linex combined process (Figure 1). This method is designed for the continuous pressing of non-ferrous metals and alloys. Its key difference from the classic Linex process is the

possibility of deformation without significantly changing the initial dimensions of the workpiece.

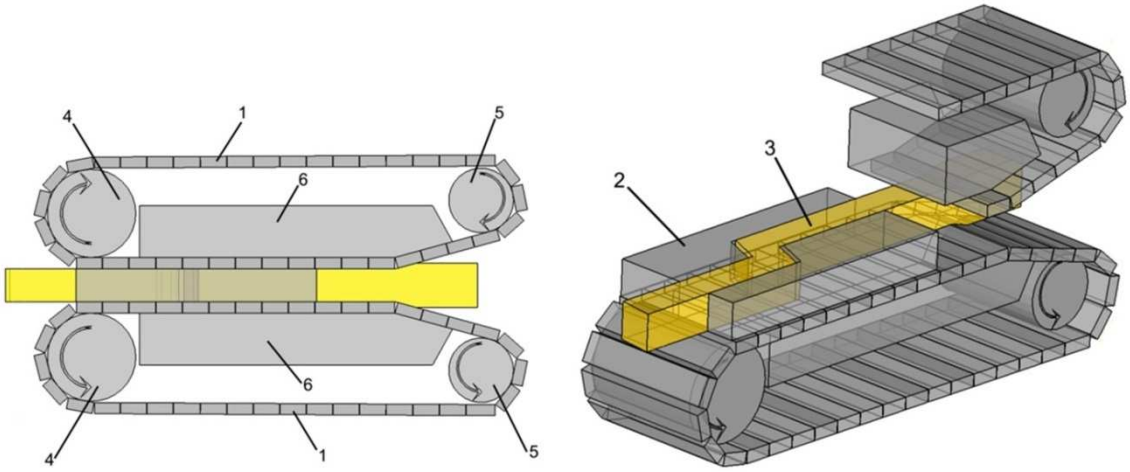

Fig. 1 *ECAP – Linex combined process: 1 - movable belt blocks, 2 – ECAP matrix, 3 – blank, 4 – idle pulleys, 5 - drive pulleys, 6 - fixed locking blocks*

Deformation in this device is carried out as follows. The workpiece is fed to the device, where movable chain blocks grab the workpiece and push it through the channels of the fixed matrix. Each chain gripping block is clad on two pulleys, one of which is idle, and the other is driven by an electric motor. Due to this, the chain-gripping blocks are set in motion. The horizontal forming of the chain gripping blocks is created due to their movement along the workpiece and fixed locking blocks that perform a clamping role.

The most important stage before developing the practical implementation of any deformation process is its theoretical study, which is usually carried out for preliminary assessment of the emerging energy-power parameters. By adjusting their values, it is possible to achieve conditions for the stable course of the deformation process, i.e., such conditions under which the deformation will take place without forced stops caused by the jamming of the workpiece in the tool.

2. ANALYTICAL DEFINITION OF FORCES

In the ECAP – Linex process, the key element of deformation is an equal-channel angular matrix with parallel channels. Chain conveyors perform a dual role. Firstly, they advance the workpiece along the channels of the matrix due to adhesion to the workpiece. Secondly, they deform the workpiece by some compression in height, due to which the main level of active friction forces develops, contributing to the advancement of the workpiece through the channels of the matrix. Therefore, for the stable course of the deformation process according to the proposed scheme, it is necessary to comply with the condition:

$$P_{CONV} > P_{MATR} \tag{1}$$

where P_{CONV} represents the force created by the chain conveyor; and P_{MATR} backpressure force created by the matrix.

Let's consider each of these efforts separately. To find the backpressure force created by the matrix, it is advisable to use the equation of the pressing force in this matrix, which is obtained in [28]:

$$P_{PRESS} = 2\sigma_S \mu_2 \left[(2l_1 + l_2)(b_1 + h_1) + 2h_1^2 tg\frac{\varphi}{2} + \frac{tg\varphi \cdot h_1}{\sqrt{3}\mu_2} \right] \quad \textbf{(2)}$$

where h_1 is the workpiece height, *mm*; b_1, workpiece width, *mm*; l_1, the length of the first channel in the matrix, *mm*; l_2, the length of the second channel in the matrix, *mm*; μ_2, friction coefficient in the matrix; σ_S, metal resistance to plastic deformation (can be taken as yield strength), *MPa*; φ, angle of intersection of matrix channels, *rad*.

Here, the authors of [28] assumed that the input and output channels have the same length. If this condition is not met, equation (2) takes the form:

$$P_{PRESS} = 2\sigma_S \mu_2 \left[(l_1 + l_2 + l_3)(b_1 + h_1) + 2h_1^2 tg\frac{\varphi}{2} + \frac{tg\varphi \cdot h_1}{\sqrt{3}\mu_2} \right] \quad \textbf{(3)}$$

This equation characterizes the theoretical maximum force that occurs when the workpiece is in all three channels of the matrix. In real conditions of pressing, it is always smaller because the volume of metal in the first channel is constantly decreasing, when the punch moves.

In the developed ECAP – Linex process, only curly elements forming a channel are present in this matrix design. There are no side walls since their role is performed by the elements of the chain conveyor. Therefore, equation (3) in relation to the curly elements of the matrix takes the form:

$$P_{MATR} = 2\sigma_S \mu_2 h_1 \left[(l_1 + l_2 + l_3) + 2h_1 tg\frac{\varphi}{2} + \frac{tg\varphi}{\sqrt{3}\mu_2} \right] \quad \textbf{(4)}$$

To find the force generated by the chain conveyor, it is necessary to consider in more detail the area where the workpiece receives compression. Here, two rational schemes of chain movement along the locking block are possible – angular and radial (Figure 2).

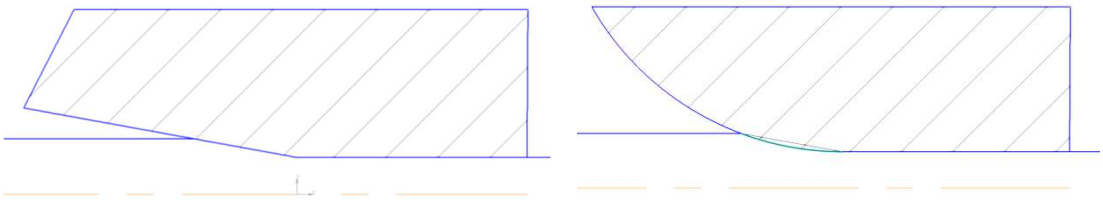

a) b)

Fig. 2 *Compression section of chain conveyor*

The most optimal option would be a radial design since in this case there are no lower corners in the contact zone of the workpiece and the tool. When the chain elements move along the fixed locking element, they hit an angle and clamps form on the workpiece surface, in the radial version such clamps are minimal or completely absent, which depends on the width of the chain element links. At the same time, it should be noted that in both cases the curve lengths bounding the deformation zone are commensurate, the difference in their lengths is about *0.5%*. Therefore, for calculation convenience, it is possible to take the shape of this deformation zone for a rolling-type shape formed by rolls. In this case, the deformation zone can be represented as follows (Figure 3).

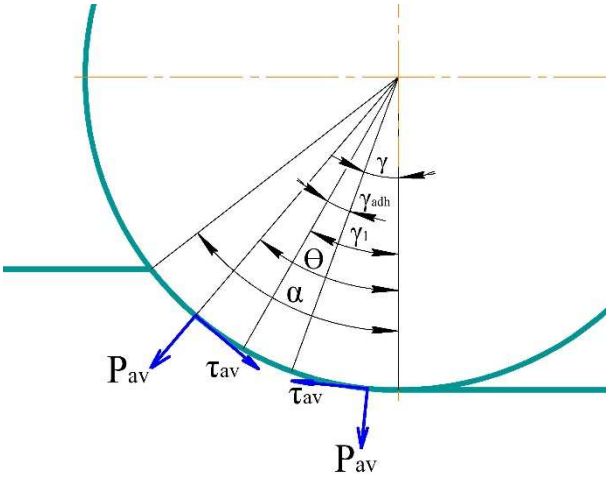

Fig. 3 *Deformation zone in the conveyor*

The sum of all the forces acting in the deformation zone is determined by the equation [28]:

$$P_{COMPR} = 2b_{av}\int_{\gamma_1}^{\alpha}\tau_{av}R\cos\theta d\theta - 2b_{av}\int_{0}^{\gamma}\tau_{av}R\cos\theta d\theta - 2b_{av}\int_{0}^{\alpha}p_{av}R\sin\theta d\theta \quad \textbf{(5)}$$

where b_1 and b_{av} represent workpiece width after compression and the average width; τ_{av} and p_{av}, the average tangential and normal stresses; R, the curvature radius of the locking block (analogous to the radius of the rolls); θ, current angle; α, capture angle; γ, γ_1, angles characterizing the advance and lag zones, respectively. Equation (5) is integrated considering the assumption that $b_{av} = b_1$:

$$P_{COMPR} = 2b_1R\tau_{av}(\sin\alpha - \sin\gamma_1) - 2b_1R\tau_{av}(\sin\gamma - 0) - 2b_1Rp_{av}(-\cos\alpha + 1) \quad \textbf{(6)}$$

Using the following relations 1-cos $\alpha = \alpha^2/2$; $\sin\alpha = \alpha$; $\sin\gamma = \gamma$; $\sin\gamma_1 = \gamma_1$; $\tau_{AV} = p_{AV}\mu = \sigma_{AV}\mu$, equation (6) becomes:

$$P_{COMPR} = 2b_1R\sigma_S\mu_1(\alpha - \gamma_1) - 2b_1R\sigma_S\mu_1\gamma - 2b_1R\sigma_S\frac{\alpha^2}{2} \quad \textbf{(7)}$$

where μ_1 is the friction coefficient in the deformation zone. The final form of the equation reads:

$$P_{COMPR} = 2b_1R\sigma_S\mu_1\left(\alpha - \gamma_1 - \gamma - \frac{\alpha^2}{2\mu_1}\right) \quad \textbf{(8)}$$

It can be seen from equation (8) that under equal geometric conditions in the deformation zone, the magnitude of the compression force depends on the values of the angles γ and γ_1, which depend on the magnitude of the backpressure force created by the matrix. For the same compression angle α, there are different zones of advance, lag, and adhesion each time. Therefore, to use equation (8), it is necessary to find the values of these angles.

The equations of equilibrium of forces and moments acting in a symmetrical deformation zone during rolling with front support, which arises due to an additional shape change in the matrix installed behind the rolls, have the form:

$$2b_{av}\int_{\gamma_1}^{\alpha}\tau_{av}R\cos\theta d\theta - 2b_{av}\int_{0}^{\gamma}\tau_{av}R\cos\theta d\theta - 2b_{av}\int_{0}^{\alpha}p_{av}R\sin\theta d\theta - \sigma_1 b_1 h_1 = 0 \quad (9)$$

$$2b_{av}\tau_{av}R^2(\alpha-\gamma_1) - 2b_{av}\tau_{av}R^2\gamma - -2b_{av}\psi R\alpha * \\ * \left(\int_{0}^{\alpha}p_{av}R\cos\theta d\theta + \int_{\gamma 1}^{\alpha}\tau_{av}R\sin\theta d\theta - \int_{0}^{\gamma}\tau_{av}R\sin\theta d\theta\right) - \sigma_1 b_1 h_1 R = 0 \quad (10)$$

where σ_1 is backpressure stress; ψ *is* the coefficient of the shoulder position of the resultant metal pressure on the rolls, while $\alpha\gamma$ are respectively the capture angle and the angle characterizing the length of the advance zone. Under the assumption $b_{av} = b_1$ the following is obtained:

$$\int_{\gamma 1}^{\alpha}\tau_{av}\cos\theta d\theta + \int_{0}^{\gamma}\tau_{av}\cos\theta d\theta - \int_{0}^{\alpha}p_{av}\sin\theta d\theta - \frac{\sigma_1 h_1}{2R} = 0 \quad (11)$$

$$\tau_{av}(\alpha-\gamma_1) - \tau_{av}\gamma - \psi\alpha\left(\int_{0}^{\alpha}p_{av}R\cos\theta d\theta + \int_{\gamma 1}^{\alpha}\tau_{av}\sin\theta d\theta - \int_{0}^{\gamma}\tau_{av}\sin\theta d\theta\right) - \frac{\sigma_1 h_1}{2R} = 0 \quad (12)$$

Integrating equation (11) and replacing 1-cos $\alpha = \alpha^2/2$; sin $\alpha = \alpha$; sin $\gamma = \gamma$; sin $\gamma_1 = \gamma_1$; $\gamma_1 = \gamma_{ADH} + \gamma$, after the transformations, the dependence for determining the angle characterizing the extent of the adhesion zone are:

$$\gamma_{ADH} = \alpha - 2\gamma - \frac{p_{AV}\alpha^2}{2\tau_{AV}} - \frac{\sigma_1 h_1}{2\tau_{AV}R} \quad (13)$$

Using $p_{AV}/\tau_{AV} = 1/\mu_1$; $\tau_{AV} = \sigma_S\mu_1$, equation (13) becomes:

$$\gamma_{ADH} = \alpha - 2\gamma - \frac{\alpha^2}{2\mu} - \frac{\sigma_1 h_1}{2\mu\sigma_S R} \quad (14)$$

After integration and transformation of equation (12):

$$\alpha - \gamma_1 - \gamma = \psi\alpha\left(\frac{p_{av}}{\tau_{av}}\alpha - \cos\alpha + \cos\gamma_1 + \cos\gamma - 1\right) + \frac{\sigma_1 h_1}{2\tau_{av}R} \quad (15)$$

The transformation of the resulting expression into a quadratic equation is obtained by performing substitutions similar to those used in solving equation (11):

$$2\gamma^2 - \gamma\left(2\alpha - \frac{\alpha^2}{\mu_1} - \frac{\sigma_1 h_1}{2\mu\sigma_S R}\right) + \frac{\alpha}{\mu_1}\left(\frac{1}{\psi} - 2 - \alpha^2 + \frac{\alpha^3}{4\mu_1} - \frac{\sigma_1 h_1}{\sigma_S R} + \frac{\alpha\sigma_1 h_1}{2\mu_1\sigma_S R} + \frac{\sigma_1^2 h_1^2}{4\mu_1\sigma_S^2 R^2\alpha}\right) = 0 \quad (16)$$

One of the roots of the quadratic equation (16) is the angle characterizing the length of the advance zone:

$$\gamma = \frac{\left(2\alpha - \frac{\alpha^2}{\mu_1} - \frac{\sigma_1 h_1}{2\mu_1 \sigma_S R}\right)}{4} - \frac{\sqrt{\left(2\alpha - \frac{\alpha^2}{\mu_1} - \frac{\sigma_1 h_1}{2\mu_1 \sigma_S R}\right)^2 - 8\frac{\alpha}{\mu_1}\left(\frac{1}{\psi} - 2 - \alpha^2 + \frac{\alpha^3}{4\mu_1} - \frac{\sigma_1 h_1}{\sigma_S R} + \frac{\alpha\sigma_1 h_1}{2\mu_1\sigma_S R} + \frac{\sigma_1^2 h_1^2}{4\mu_1\sigma_S^2 R^2 \alpha}\right)}}{4}. \quad (17)$$

In order to find this angle characterizing the advance zone according to equation (16), it is necessary to first determine the coefficient of the shoulder position of the resultant ψ. To perform this, the following conditions that ensure acceptable solution of the equation (16) are considered:

$$\left(2\alpha - \frac{\alpha^2}{\mu_1} - \frac{\sigma_1 h_1}{2\mu_1 \sigma_S R}\right)^2 > 8\frac{\alpha}{\mu_1}\left(\frac{1}{\psi} - 2 - \alpha^2 + \frac{\alpha^3}{4\mu_1} - \frac{\sigma_1 h_1}{\sigma_S R} + \frac{\alpha\sigma_1 h_1}{2\mu_1\sigma_S R} + \frac{\sigma_1^2 h_1^2}{4\mu_1\sigma_S^2 R^2 \alpha}\right) \quad (18)$$

$$\frac{1}{\psi} - 2 - \alpha^2 + \frac{\alpha^3}{4\mu_1} - \frac{\sigma_1 h_1}{\sigma_S R} + \frac{\alpha\sigma_1 h_1}{2\mu_1\sigma_S R} + \frac{\sigma_1^2 h_1^2}{4\mu_1\sigma_S^2 R^2 \alpha} > 0 \quad (19)$$

Solving both inequalities (18) and (19) the following limits for $1/\psi$ are obtained:

$$\frac{\mu_1}{8\alpha}\left(2\alpha - \frac{\alpha^2}{\mu_1} - \frac{\sigma_1 h_1}{2\mu_1 \sigma_S R}\right)^2 + 2 + \alpha^2 - \frac{\alpha^3}{4\mu_1} + \frac{\sigma_1 h_1}{\sigma_S R} - \frac{\alpha\sigma_1 h_1}{2\mu_1\sigma_S R} - \frac{\sigma_1^2 h_1^2}{4\mu_1\sigma_S^2 R^2 \alpha} > \frac{1}{\psi} > 2 + \alpha^2 - \frac{\alpha^3}{4\mu_1} + \frac{\sigma_1 h_1}{\sigma_S R} - \frac{\alpha\sigma_1 h_1}{2\mu_1\sigma_S R} - \frac{\sigma_1^2 h_1^2}{4\mu_1\sigma_S^2 R^2 \alpha} \quad (20)$$

Assuming that the value $1/\psi$ is in the middle part of the indicated limits:

$$\frac{1}{\psi} = \frac{\mu_1}{16\alpha}\left(2\alpha - \frac{\alpha^2}{\mu_1} - \frac{\sigma_1 h_1}{2\mu_1 \sigma_S R}\right)^2 + 2 + \alpha^2 - \frac{\alpha^3}{4\mu_1} + \frac{\sigma_1 h_1}{\sigma_S R} - \frac{\alpha\sigma_1 h_1}{2\mu_1\sigma_S R} - \frac{\sigma_1^2 h_1^2}{4\mu_1\sigma_S^2 R^2 \alpha} \quad (21)$$

Knowing the magnitude of the angles characterizing the extent of the advance and adhesion zones, the angle characterizing the lag zone can be found as:

$$\gamma_{lag} = \alpha - \gamma_{adh} - \gamma \quad (22)$$

However, in this combined process, the useful force pushing the workpiece through the channels of the matrix is expressed not only by the equation (8). Here, in addition to the compression force, there is also a force from the friction of the workpiece on the chain element links, since their movement is directed in the same direction as the movement of the workpiece. Therefore, the maximum possible force generated by the conveyor at the moment when the workpiece completely fills all the channels of the matrix is:

$$P_{CONV} = 2b_1\sigma_S\mu_1\left[R\left(\alpha - \gamma_1 - \gamma - \frac{\alpha^2}{2\mu_1}\right) + (l_1 + l_2 + l_3)\right] \quad (23)$$

The force of advancing the workpiece by one link of the chain element is equal to:

$$P_{1\_EL} = 2\sigma_S\mu_1 b_1 l_{EL} \quad (24)$$

where l_{EL} is single link length of chain element.

3. RESULTS AND DISCUSSION

A trial calculation is performed with the following initial data: $R=50$ *mm*, $b_1=10$ *mm*, $h_1=10$ *mm*, workpiece compression $\Delta h=3$ *mm*, $\mu_1=0,7$, $\mu_2=0,08$, $l_1=30$ *mm*, $l_2=20$ *mm*, $l_3=15$ *mm*, $\sigma_S=55$ *MPa* (yield strength of rod aluminum alloy AD31 (analog of Al6061) without preliminary heat treatment according to GOST 21488-97, heated to *150°C* [29, 30]). Values of friction coefficients are assumed as recommended by Deform and Simufact Forming systems for polished surfaces with lubricant (matrix) and rough surfaces without lubricant (pulley). When entering the algorithm into Microsoft Excel and varying the value of the channel junction angle in the matrix from *90°* to *180°*, the following data are obtained (Figure 4).

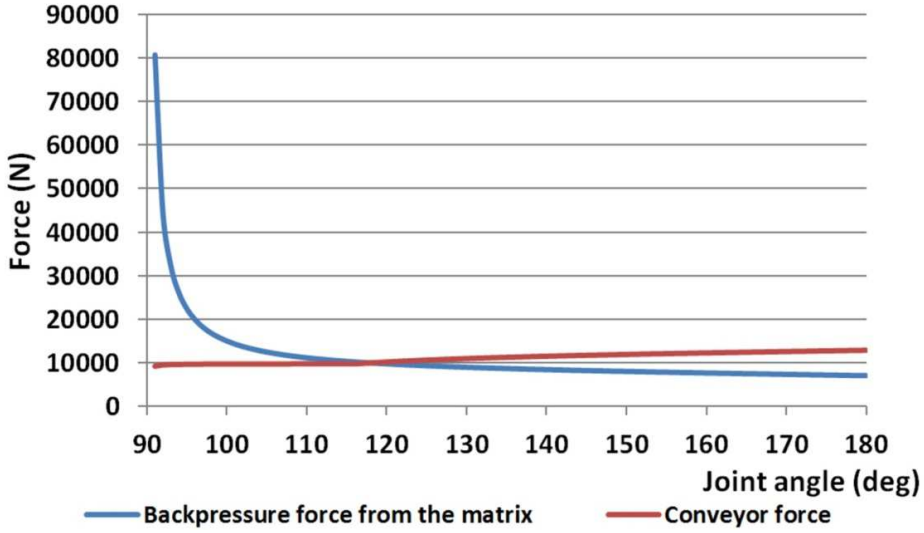

Fig. 4 *Dependences of the forces of the ECAP – Linex process on the value of the channel junction angle*

Since the deformation scheme under consideration is inherently close to the previously mentioned rolling-ECAP scheme, it is advisable to conduct a comparative analysis of these technologies. For this purpose, a similar graph of forces is drawn (Figure 5). The purpose of the comparative analysis is to assess the emerging forces with the same initial data.

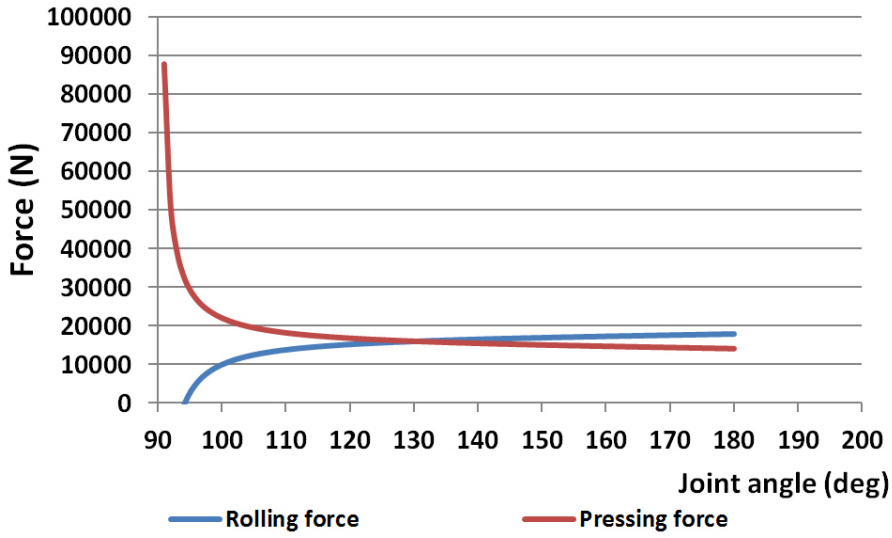

Fig. 5 *Dependence of the forces of the rolling-ECAP process on the value of the channel junction angle*

Analyzing the obtained graphs, the following characteristics can be noted:

1) The graphs of the backpressure force and the pressing force have an exponential character, i.e., with a decrease in the angle, the force values increase exponentially. At the same time, the absolute value of the force in the process of ECAP – Linex is lower by about *40-50%* for the gentlest section of the joint angle values from *120°* to *180°*.

2) The force generated by the conveyor has a flatter appearance than the rolling force. This is explained by the fact that in addition to the direct compression force in the deformation zone, there is also a component of the force from the friction of the workpiece on the chain element links. Due to this, the force still depends on the angle of the junction of the channels, but not as obviously as in the rolling-ECAP process.

3) With the given initial data, the ECAP –Linex process is stable at a channel junction angle of less than *120°*, while the rolling-ECAP process is stable at a channel junction angle of less than *132°*. This factor suggests that during the implementation of the ECAP – Linex process, a higher level of active friction forces is created, contributing to the advancement of the workpiece through the matrix channels. Therefore, in this case, it is possible to use a matrix with a steeper angle, which increases the level of metal processing at the pressing stage.

4) The overall level of effort in the "ECAP–Linex" process is lower than in the rolling-ECAP process. This allows us to talk about the increased durability of the tool when implementing this combined process in practice.

To confirm the conclusions made, additional calculations are made for various sections of square and rectangular sections. For comparison, the limits of a stable process are determined, i.e., the angle at which the forces for each process are equalized. In each algorithm, the values of the height and width of the workpiece are changed, but the other parameters are not. The results of the calculations are summarized in Table 1.

Table 1 *Summary values of forces for workpieces of various sections made of aluminum alloy 6061*

h x b, mm	*ECAP–Linex*		*rolling-ECAP*	
	$P_{CONV} = P_{MATR}$, *N*	*Angle φ, deg*	$P_{ROLL} = P_{PRESS}$, *N*	*Angle φ, deg*
10 x 10	*9970*	*120*	*15940*	*132*
10 x 15	*13420*	*112*	*23750*	*118*
15 x 15	*15090*	*122*	*24220*	*136*
15 x 20	*20130*	*114*	*32370*	*120*

The data in Table 1 confirm the conclusions. In addition, it can be noted that with an increase in the workpiece width with a constant height, the total equalizing force increases, but the required angle value decreases. This is because the process in both cases proceeds stably only if condition (1) is met. Therefore, with an increase in the workpiece width, it is the rolling force (conveyor) that increases more intensively. With an increase in the workpiece height, the required force and the angle of the joint increase. However, for the same workpiece section, the required force values and the joint angle are significantly lower for the ECAP – Linex process.

To verify the correctness of the obtained values according to the equations, verification using computer simulation by the finite element method in Deform v.13 is carried out. This program is widely used for the simulation of various metal forming, heat treatment, and machining processes. To create a model of the ECAP-Linex process, geometric and technological parameters specified in the trial calculation are used.

When creating a FEM model of this process, it is necessary to correctly set the speed parameters of the deforming elements. According to the principle of the Linex process [31], chain elements receive movement from rotating pulleys, when passing along the contour of fixed blocks, they grab the workpiece, compress it and push it through the channels of the matrix. Since the linear velocity of the chain element links is equal to the linear velocity on the surface of the rotating pulleys, it is most appropriate to simulate the movement of chain elements as follows. The rotating pulley is created with the curvature radius of the fixed block (green zone in Figure 2b). At the exit from the vertical axis of the rotation of the pulley, the shaped elements of the matrix are located. On the upper face of the matrices, the horizontal line of which corresponds to the lower point level of the pulley radius, single links are created sequentially (the length of the links should be small, for a given radius of the pulley *50 mm*, it is adopted *5 mm*). Considering the rotation speed of the pulleys of *15 rpm* (*1.57 rad/s*) and a radius of *50 mm*, the linear speed of the links is *78.5 mm/s*.

To increase the calculation speed, it is decided to use horizontal symmetry, i.e., ½ of the thickness of the workpiece is modeled. According to this condition, the initial blank had a width of *9 mm*, a height of *6.5 mm*, and a length of *75 mm*. Al6061 alloy is used as workpiece material, and flow stress curves are used from Deform materials library. The workpiece volume is divided into *45,000* finite elements of the tetrahedral form with a volume difference factor of 3, i.e., the biggest element by volume is 3 times larger than the smallest. So, the biggest finite element has a length of *1.8 mm*, and the smallest finite element has a length of *0.6 mm*. Also, an option for volume loss compensation is activated. The difference between the initial and FE volume is less than *0.5%*. Remeshing options are set as default. For this model, it is decided to use a channel junction angle of *140°*. Ziebel model is used as friction law. It is found that the process proceeds stably with the above parameters (Figure 6).

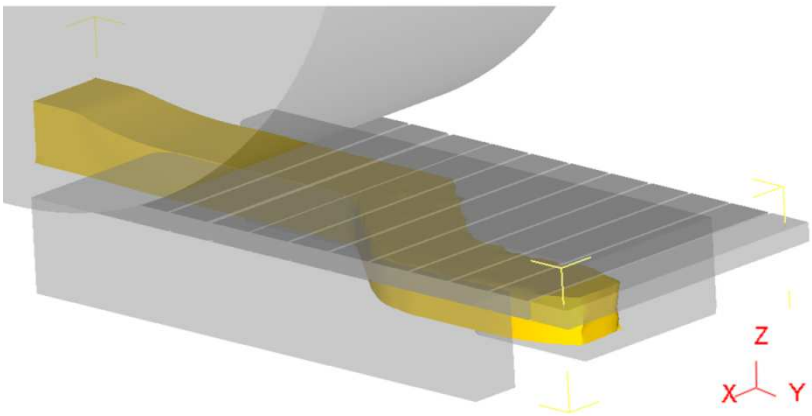

Fig. 6 *Simulation result corresponding to the final stage*

Based on the simulation results, the following force graphs for the pulley, matrix, and chain element link are obtained (Figure 7).

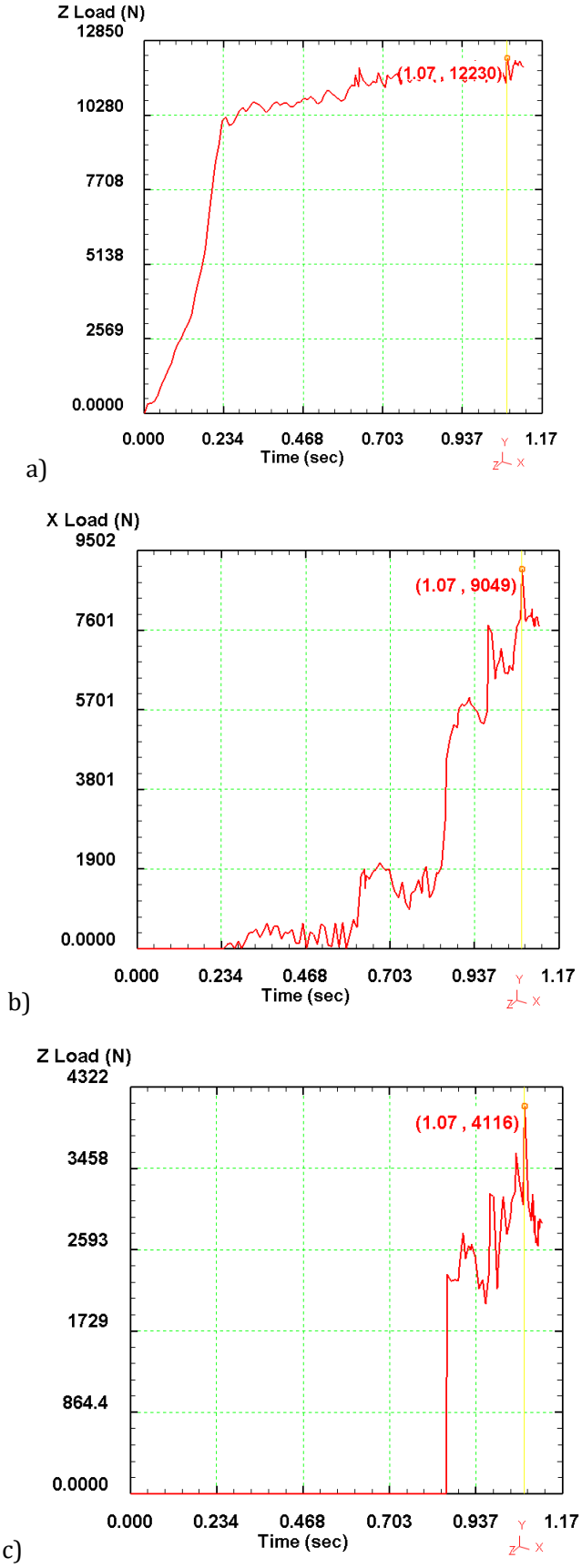

Fig. 7 *Forces obtained by FEM simulation: a) – pulley; b) – matrix; c) – link*

Obtained graphs are constructed by axes where maximal normal stresses occur; this is usually the perpendicular direction (axes direction in Figure 6). Thus, graphs for the pulley and link have a Z axis, and the graph for the matrix has an X axis. The view of the pulley graph (Figure 7a) is typical for the rolling process, where the deformation zone is filled by metal (capture stage), after that the process becomes stable and the force graph has a more horizontal view. At the same time, the view of the matrix graph (Figure 7b) is typical for the pressing process in chosen matrix type – the graph has two steps that indicate two angle joints. After each step, the value of force increases. The graph for the link (Figure 7c) has two zones. The first half has a zero-force value that indicates a lack of decompression. But when metal is filled the second angle joint, the backpressure is increased and decompression occurs. It leads to an increased force value on the link.

Table 2 shows the force values obtained by analytical approach and by FEM simulation. Comparison of values showed high convergence for all three cases.

Table 2 *Forces obtained by analytical and FEM approach*

	Analytical - force, N	*FEM - force, N*	*Difference, %*
Pulley	*12542*	*12230*	*2,48*
Matrix	*9192*	*9049*	*1,55*
Link	*4200*	*4116*	*2*

4. CONCLUSION

Theoretical studies of the combined process ECAP-Linex are carried out. To analyze the resulting deformation forces, the stages of pressing in a matrix and compression by a chain conveyor are separately considered. The obtained equations are used during the trial calculation. A comparative analysis with the previously known rolling-ECAP process showed that the new ECAP-Linex process allows for a stable deformation process with lower forces and a smaller channel junction angle in the matrix, which leads to an increase in the level of metal processing at the pressing stage. Verification of the values obtained by equations with computer simulation using the finite element method in the Deform program showed that the values of the forces in the calculation and modeling have a high level of convergence, and for all three considered details, the difference did not exceed *3%*. Further study of this combined process involves computer modeling with varying values of key geometric and technological parameters of the process. The assessment of the stress-strain state and the deformation force allows for determining the most optimal parameters that are the basis for the design of a laboratory installation.

5. ACKNOWLEDGEMENTS

This research was funded by the Science Committee of the Ministry of Education and Science of the Republic of Kazakhstan (Grant № AP13067723).

6. REFERENCES

[1] M. Jahedi, M. Knezevic, M.H. Paydar, High-Pressure Double Torsion as a Severe Plastic Deformation Process: Experimental Procedure and Finite Element Modeling, *Journal of Materials Engineering and Performance*, Vol. 24, pp. 1471-1482, 2015.

https://doi.org/10.1007/s11665-015-1426-0

[2] J. Straska, M. Janecek, J. Gubicza, T. Krajnak, E.Y. Yoon, H.S. Kim, Evolution of microstructure and hardness in AZ31 alloy processed by high pressure torsion, *Materials Science & Engineering A: Structural Materials: Properties, Microstructure and Processing*, Vol. 625, pp. 98-106, 2015. https://doi.org/10.1016/j.msea.2014.12.005

[3] A. Alhamidi, Z. Horita, Grain refinement and high strain rate superplasticity in alumunium 2024 alloy processed by high-pressure torsion, *Materials Science & Engineering A: Structural Materials: Properties, Microstructure and Processing*, Vol. 622, pp. 139-145, 2015. https://doi.org/10.1016/j.msea.2014.11.009

[4] M.H. Shaeri, M.T. Salehi, S.H. Seyyedein, M.R. Abutalebi, J.K. Park, Microstructure and mechanical properties of Al-7075 alloy processed by equal channel angular pressing combined with aging treatment, *Materials and Design*, Vol. 57, pp. 250-257, 2014.

https://doi.org/10.1016/j.matdes.2014.01.008

[5] X. Zhang, X. Liu, J. Wang, Y. Cheng, Effect of route on tensile anisotropy in equal channel angular pressing, *Materials Science & Engineering A: Structural Materials: Properties, Microstructure and Processing*, Vol. 676, pp. 65-72, 2016.

https://doi.org/10.1016/j.msea.2016.08.108

[6] W. Wei, S.L. Wang, K.X. Wei, I.V. Alexandrov, Q.B. Du, J. Hu, Microstructure and tensile properties of Cu-Al alloys processed by ECAP and rolling at cryogenic temperature, *Journal of Alloys and Compounds*, Vol. 678, pp. 506-510, 2016.

https://doi.org/10.1016/j.jallcom.2016.04.035

[7] E. Mostaed, A. Fabrizi, F. Bonollo, M. Vedani, Microstructural, texture, plastic anisotropy and superplasticity development of ZK60 alloy during equal channel angular extrusion processing, *Metallurgia Italiana*, Vol. 11-12, pp. 5-12, 2015.

[8] R. Kaibyshev, D. Zhemchuzhnikova, A. Mogucheva, Effect of Mg Content on High Strain Rate Superplasticity of Al-Mg-Sc-Zr Alloys Subjected to Equal-Channel Angular Pressing, *Materials Science Forum*, Vol. 735, pp. 265-270, 2013.

https://doi.org/10.4028/www.scientific.net/MSF.735.265

[9] C. Banjongprasert, A. Jak-Ra, C. Domrong, U. Patakham, W. Pongsaksawad, T. Chairuangsri, Characterization of an Equal Channel Angular Pressed Al-Zn-In Alloy, *Archives of Metallurgy and Materials*, Vol. 60, pp. 887-890, 2015.

https://doi.org/10.1515/amm-2015-0224

[10] V.I. Betekhtin, J. Dvorak, A.G. Kadomtsev, B.K. Kardashev, M.V. Narykova, G.K. Raab, V. Sklenicka, S.N. Faizova, Durability and static strength of microcrystalline titanium VT1-0 obtained by equal-channel angular pressing, *Technical Physics Letters*, Vol. 41, pp. 80-82, 2015. https://doi.org/10.1134/S1063785015010228

[11] Y. Liu, Z.X. Kang, L.L. Zhou, J.Y. Zhang, Y.Y. Li, Mechanical properties and biocorrosion behaviour of deformed Mg-Gd-Nd-Zn-Zr alloy by equal channel angular pressing, *Corrosion Engineering Science and Technology*, Vol. 51, pp. 256-262, 2016.

https://doi.org/10.1179/1743278215Y.0000000050

[12] O.E. Markov, A.V. Perig, M.A. Markova, V.N. Zlygoriev, Development of a new process for forging plates using intensive plastic deformation, *International Journal of Advanced Manufacturing Technology*, Vol. 83, pp. 2159-2174, 2016.

https://doi.org/10.1007/s00170-015-8217-5

[13] V. Kukhar, E. Balalayeva, S. Hurkovska, Y. Sahirov, O. Markov, A. Prysiazhnyi, O. Anishchenko, The selection of options for closed-die forging of complex parts using computer simulation by the criteria of material savings and minimum forging force, *Advances in Intelligent Systems and Computing*, Vol. 989, pp. 325-331, 2020.

https://doi.org/10.1007/978-981-13-8618-3_35

[14] V.V. Drahobetsky, A.A. Shapoval, V.T. Shchetynin, R.G. Argat, S.V. Shlyk, D.V. Mos'pan, S.M. Gorbatyuk, O.E. Markov, New Solution for Plastic Deformation Process Intensification, *Metallurgist*, Vol. 65, pp. 1108-1116, 2022.

https://doi.org/10.1007/s11015-022-01253-x

[15] O.E. Markov, A.S. Khvashchynskyi, A.V. Musorin, M.A. Markova, A.A. Shapoval, NS. Hrudkina, Investigation of new method of large ingots forging based on upsetting of workpieces with ledges, *International Journal of Advanced Manufacturing Technology*, Vol. 122, pp. 1383-1394, 2022. https://doi.org/10.1007/s00170-022-09989-1

[16] O.E. Markov, O.V. Gerasimenko, A.A. Shapoval, O.R. Abdulov, R.U. Zhytnikov, Computerized simulation of shortened ingots with a controlled crystallization for manufacturing of high-quality forgings, *International Journal of Advanced Manufacturing Technology*, Vol. 103, pp. 3057-3065, 2019. https://doi.org/10.1007/s00170-019-03749-4

[17] Y. Estrin, A. Vinogradov, Extreme grain refinement by severe plastic deformation: A wealth of challenging science, *Acta Materialia*, Vol. 61, pp. 782-817, 2013.

https://doi.org/10.1016/j.actamat.2012.10.038

[18] T. Sakai, A. Belyakov, R. Kaibyshev, H. Miura, J.J. Jonas, Dynamic and post-dynamic recrystallization under hot, cold and severe plastic deformation conditions, *Progress in Materials Science*, Vol. 60, pp. 130-207, 2014.

https://doi.org/10.1016/j.pmatsci.2013.09.002

[19] T.G. Langdon, Twenty-five years of ultrafine-grained materials: Achieving exceptional properties through grain refinement, *Acta Materialia*, Vol. 61, pp. 7035-7059, 2013.

https://doi.org/10.1016/j.actamat.2013.08.018

[20] R.Z. Valiev, Superior strength in ultrafine-grained materials produced by SPD processing, *Materials Transactions*, Vol. 55, No. 1, pp. 13-18, 2014.

https://doi.org/10.2320/matertrans.MA201325

[21] R.Z. Valiev, T.G. Langdon, Principles of equal-channel angular pressing as a processing tool for grain refinement, *Progress in Materials Science*, Vol. 51, pp. 881–981, 2006.

https://doi.org/10.1016/j.pmatsci.2006.02.003

[22] A. Naizabekov, I. Volokitina, A. Volokitin, E. Panin, Structure and Mechanical Properties of Steel in the Process "Pressing–Drawing", *Journal of Materials Engineering and Performance*, Vol. 28, No. 3, pp. 1762-1771, 2019.

https://doi.org/10.1007/s11665-019-3880-6

[23] A. Naizabekov, S. Lezhnev, E. Panin, I. Volokitina, A. Arbuz, T. Koinov, I. Mazur, Effect of Combined Rolling–ECAP on Ultrafine-Grained Structure and Properties in 6063 Al Alloy, *Journal of Materials Engineering and Performance*, Vol. 28, No. 1, pp. 200–210, 2019.

https://doi.org/10.1007/s11665-018-3790-z

[24] A. Naizabekov, S. Lezhnev, A. Arbuz, E. Panin, Combined process "helical rolling-pressing" and its effect on the microstructure of ferrous and non-ferrous materials, *Metallurgical Research & Technology*, Vol. 115, No. 2, article number 213, 2018.

https://doi.org/10.1051/metal/2017099

[25] J. Bartnicki, Numerical analysis of rolling extrusion process of a hollow hub, *Archives of Metallurgy and Materials*, Vol. 57, pp. 1137-1142, 2012.

https://doi.org/10.2478/v10172-012-0127-z

[26] E.S. Lopatina, V.S. Biront, S.B. Sidelnikov, Metallographic tests of modifying ability of rods from aluminum alloys obtained by combined casting and rolling-extruding, *Journal of Siberian Federal University. Engineering and Technologies*, Vol. 7, No. 2, pp. 127-131, 2014.

[27] E.A. Panin, A.B. Naizabekov, A.V. Volokitin, G.E. Akhmetova, I.E. Volokitina, A.O. Tolkushkin, New concepts of severe plastic deformation combined processes, *Industry 4.0*, Vol. 7, No. 2, pp. 59-61, 2022.

[28] A. Naizabekov, S. Lezhnev, E. Panin, T. Koinov, Theoretical grounds of the combined "rolling - equal - channel step pressing" process, *Journal of Chemical Technology and Metallurgy*, Vol. 51, No. 5, pp. 594-602, 2016.

[29] GOST 21488-97, Rods pressed from aluminum and aluminum alloys.

[30] I. Sabirov, M.T. Perez-Prado, M. Murashkin, J.M. Molina-Aldareguia, E.V. Bobruk, N.F. Yunusova, R.Z. Valiev, Application of equal channel angular pressing with parallel channels for grain refinement in aluminium alloys and its effect on deformation behavior, *International Journal of Material Forming*, Vol. 3, pp. 411-144, 2010.

https://doi.org/10.1007/s12289-010-0794-0

[31] W.G. Voorhes, Extrusion process, US Patent 3922898A, 1975.